

Boosting Adversarial Training with Hypersphere Embedding

Tianyu Pang ^{*1} Xiao Yang ^{*1} Yinpeng Dong ¹ Kun Xu ¹ Hang Su ¹ Jun Zhu ¹

Abstract

Adversarial training (AT) is one of the most effective defenses to improve the adversarial robustness of deep learning models. In order to promote the reliability of the adversarially trained models, we propose to boost AT via incorporating hypersphere embedding (HE), which can regularize the adversarial features onto compact hypersphere manifolds. We formally demonstrate that AT and HE are well coupled, which tunes up the learning dynamics of AT from several aspects. We comprehensively validate the effectiveness and universality of HE by embedding it into the popular AT frameworks including PGD-AT, ALP, and TRADES, as well as the FreeAT and FastAT strategies. In experiments, we evaluate our methods on the CIFAR-10 and ImageNet datasets, and verify that integrating HE can consistently enhance the performance of the models trained by each AT framework with little extra computation. Code is available at https://github.com/ShawnXYang/AT_HE.

1. Introduction

The adversarial vulnerability of deep learning models has been widely recognized in recent years (Biggio et al., 2013; Szegedy et al., 2014; Goodfellow et al., 2015). To mitigate this potential threat, a number of defenses have been proposed, but most of them are ultimately defeated by the attacks adapted to the specific details of the defenses (Carlini & Wagner, 2017b; Athalye et al., 2018). Among the existing defenses, **adversarial training (AT)** is a general strategy achieving the state-of-the-art robustness under different settings (Tramèr et al., 2018; Madry et al., 2018; Xie et al., 2019; Zhang et al., 2019b; Wu et al., 2020).

Various efforts have been devoted to improving AT from different aspects, including accelerating the training proce-

^{*}Equal contribution ¹Dept. of Comp. Sci. & Tech., BNRIst Center, Institute for AI, THBI Lab, Tsinghua University. Correspondence to: Tianyu Pang <pty17@mails.tsinghua.edu.cn>, Xiao Yang <yangxiao19@mails.tsinghua.edu.cn>, Jun Zhu <dc-szj@tsinghua.edu.cn>.

dure (Shafahi et al., 2019; Zhang et al., 2019a; Wong et al., 2020) and exploiting extra labeled and unlabeled training data (Hendrycks et al., 2019; Alayrac et al., 2019; Carmon et al., 2019), which are effective in the cases with limited computational resources or additional data accessibility.

In the meanwhile, another complementary research route focuses on boosting the adversarially trained models via learning more reliable representations. Along this line, recent progress shows that encoding triplet-wise metric learning or maximizing the optimal transport distance of data batch in AT is effective to leverage the inter-sample interactions, which can learn robust classifiers (Mao et al., 2019; Zhang & Wang, 2019; Li et al., 2019; Pang et al., 2019). However, optimization on the sampled triplets or the optimal transport distance is usually of high computational cost, while the sampling process can also introduce extra class biases on unbalanced data (Parkhi et al., 2015; Schroff et al., 2015).

To improve the adaptivity and computational efficiency of learning reliable representations, we propose to augment AT by integrating **hypersphere embedding (HE)**, which enables the deep neural networks to learn angularly discriminative and more robust features, both efficiently and evenly. Our strategy can be geometrically viewed as regularizing the adversarial features into the vicinity of the clean feature manifolds constrained on a hypersphere. Extensive formal analyses show that AT and HE are well coupled to tune up the learning dynamics, which is conducive to the adversarially trained models, as detailed in Sec. 3. In other domains like face recognition (Liu et al., 2017) and unsupervised learning (Wu et al., 2018), different variants of HE have also achieved wide empirical success. Specifically, the HE mechanism in our method consists of three typical operations, i.e., **HE=FN+WN+AM**, as explained below:

Feature normalization (FN). In a deep neural network, FN normalizes the feature vectors of the penultimate layer into a fixed length, which is widely employed in deep metric learning (Wang et al., 2017b; Sun et al., 2014). It can avoid the non-effective increase of feature norm on easy examples and encourage the model to emphasize on hard examples (Wang et al., 2017a; Ranjan et al., 2017). This property of FN naturally adapts to AT since the adversarial samples crafted in training are usually considered as hard examples that the model should pay more attention to.

Weight normalization (WN). WN normalizes the weights in the softmax layer to encourage the model to equally treat samples from different classes, facilitating the cases with unbalanced training data (Guo & Zhang, 2017; Liu et al., 2017; Pang et al., 2018; 2020). Since existing AT frameworks usually apply untargeted or multi-targeted attacks (Madry et al., 2018; Gowal et al., 2019), WN can adaptively tune the training process with an erratic distribution of adversarial labels.

Angular margins (AM). When FN and WN are both applied, the inner product in the softmax layer becomes a cosine metric. We can therefore introduce AM to encourage a larger inter-class variance to learn more generalizable features (Deng et al., 2019). In the adversarial setting, it has been shown that large margins are helpful for model robustness (Elsayed et al., 2018; Yan et al., 2018), which supports our motivation to encode AM into the AT procedure.

In this paper, we mainly consider three popular AT frameworks to validate our method of incorporating HE in AT, namely, **PGD-AT** (Madry et al., 2018), **ALP** (Kannan et al., 2018), and **TRADES** (Zhang et al., 2019b), as summarized in Table 1. We further verify the universality of our method by evaluating the performance of combining HE with previous strategies on accelerating AT, e.g., **FreeAT** (Shafahi et al., 2019) and **FastAT** (Wong et al., 2020).

In Sec. 4, we empirically evaluate the defenses on CIFAR-10 (Krizhevsky & Hinton, 2009) and ImageNet (Deng et al., 2009) following the guidelines in Carlini et al. (2019). We also test on the CIFAR-10-C and ImageNet-C datasets with corrupted images to inspect the robustness under general transformations (Hendrycks & Dietterich, 2019). The results demonstrate that incorporating HE can consistently improve the performance of the models trained by each AT framework, while introducing little extra computation.

2. Methodology

In this section, we define the notations, introduce the hypersphere embedding (HE) mechanism, and provide the formulations under the adversarial training (AT) frameworks.

2.1. Notations

For a classification task with L labels in $[L] := \{1, \dots, L\}$, the deep neural network (DNN) can be generally denoted as

$$f(x) = \mathbb{S}(\mathbf{W}^\top z + b), \quad (1)$$

where x is the input, $z = z(x; \omega)$ is the extracted feature with model parameters ω , the matrix $\mathbf{W} = (W_1, \dots, W_L)$ and vector b are respectively the weight and bias in the softmax layer, and $\mathbb{S}(h) : \mathbb{R}^L \rightarrow \mathbb{R}^L$ is the softmax function defined as $\mathbb{S}(h)_i = \exp(h_i) / \sum_{l \in [L]} \exp(h_l)$ for $\forall i \in [L]$.

For an input-label pair (x, y) , one common training objective for DNNs is to minimize the cross-entropy (CE) loss

$$\mathcal{L}_{\text{CE}}(f(x), y) = -1_y^\top \log f(x), \quad (2)$$

where 1_y is the one-hot encoding of label y and the logarithm of a vector is taken element-wisely. In this paper, we use $\angle(u, v)$ to denote the angle between the vector u and v .

2.2. The AT Frameworks with HE

Adversarial training (AT) is one of the most effective and widely studied defense strategies against adversarial vulnerability (Kurakin et al., 2018; Carlini et al., 2019; Brendel et al., 2020). Most of the existing AT methods can be formulated as a two-stage framework:

$$\begin{aligned} & \min_{\omega, \mathbf{W}} \mathbb{E} [\mathcal{L}_T(\omega, \mathbf{W} | x, x^*, y)], \\ & \text{where } x^* = \arg \max_{x' \in \mathbf{B}(x)} \mathcal{L}_A(x' | x, y, \omega, \mathbf{W}). \end{aligned} \quad (3)$$

Here $\mathbf{B}(x)$ is a set of allowed points around x , \mathcal{L}_T and \mathcal{L}_A are the training and adversarial objectives, respectively. Since the inner maximization and outer minimization problems are mutually coupled, they are iteratively executed in training until the model parameters ω and \mathbf{W} converge.

To encourage the adversarially trained models to learn more reliable features, recent work proposes to embed pair-wise or triplet-wise metric learning into AT (Mao et al., 2019; Zhang & Wang, 2019; Li et al., 2019). However, these methods could introduce high computation overhead to optimize on the sampled triplets or the OT-distances, as well as cause unexpected class biases (Hoffer & Ailon, 2015).

In response to these problems, we are motivated to cast about for ways to improve the adaptivity and computational efficiency of learning reliable representations. To this end, we propose to augment AT by integrating **hypersphere embedding (HE)**, which enables the model to efficiently and evenly learn discriminative and robust features. Our strategy can be geometrically viewed as regularizing the adversarial features into the vicinity of the clean feature manifolds on a hypersphere. The implementation of HE mainly consists of three typical operations including feature normalization (FN) (Ranjan et al., 2017), weight normalization (WN) (Guo & Zhang, 2017), and angular margins (AM) (Liu et al., 2016), i.e., **HE=FN+WN+AM**, as detailed below.

Note that in Eq. (1) there is $\mathbf{W}^\top z = (W_1^\top z, \dots, W_L^\top z)$, and $\forall l \in [L]$, the inner product $W_l^\top z = \|W_l\| \|z\| \cos(\theta_l)$, where $\theta_l = \angle(W_l, z)$.¹ Then the WN operation normalizes W_l to \widetilde{W}_l , and the FN operation normalizes z to \widetilde{z} , where

$$\widetilde{W}_l = \frac{W_l}{\|W_l\|}, \quad \widetilde{z} = s \frac{z}{\|z\|}, \quad (4)$$

and s is a hyperparameter (Wang et al., 2017a). Let $\cos \boldsymbol{\theta} = (\cos(\theta_1), \dots, \cos(\theta_L))$, then the output predictions of the DNNs with HE become

$$\tilde{f}(x) = \mathbb{S}(\widetilde{\mathbf{W}}^\top \widetilde{z}) = \mathbb{S}(s \cdot \cos \boldsymbol{\theta}), \quad (5)$$

¹We omit the subscript of ℓ_2 -norm without ambiguity.

Table 1. Formulations of the AT frameworks without (✗) or with (✓) HE. The notations are defined in Sec. 2.2. We substitute the adversarial attacks in ALP with untargeted PGD, as suggested by Engstrom et al. (2018).

AT framework	HE	Training objective \mathcal{L}_T	Adversarial objective \mathcal{L}_A
PGD-AT	✗	$\mathcal{L}_{CE}(f(x^*), y)$	$\mathcal{L}_{CE}(f(x'), y)$
	✓	$\mathcal{L}_{CE}^m(\tilde{f}(x^*), y)$	$\mathcal{L}_{CE}(\tilde{f}(x'), y)$
ALP	✗	$\alpha \mathcal{L}_{CE}(f(x), y) + (1 - \alpha) \mathcal{L}_{CE}(f(x^*), y) + \lambda \ \mathbf{W}^\top(z - z^*)\ _2$	$\mathcal{L}_{CE}(f(x'), y)$
	✓	$\alpha \mathcal{L}_{CE}^m(\tilde{f}(x), y) + (1 - \alpha) \mathcal{L}_{CE}^m(\tilde{f}(x^*), y) + \lambda \ \tilde{\mathbf{W}}^\top(\tilde{z} - \tilde{z}^*)\ _2$	$\mathcal{L}_{CE}(\tilde{f}(x'), y)$
TRADES	✗	$\mathcal{L}_{CE}(f(x), y) + \lambda \mathcal{L}_{CE}(f(x^*), f(x))$	$\mathcal{L}_{CE}(f(x'), f(x))$
	✓	$\mathcal{L}_{CE}^m(\tilde{f}(x), y) + \lambda \mathcal{L}_{CE}(\tilde{f}(x^*), \tilde{f}(x))$	$\mathcal{L}_{CE}(\tilde{f}(x'), \tilde{f}(x))$

where no bias vector b exists in $\tilde{f}(x)$ (Wang et al., 2017a). In contrast, the AM operation is only performed in the training phase, where $\tilde{f}(x)$ is fed into the CE loss with a margin m . In this paper, we apply the Large Margin Cosine (LMC) Loss (Wang et al., 2018) with an additive margin as

$$\mathcal{L}_{CE}^m(\tilde{f}(x), y) = -1_y^\top \log \mathbb{S}(s \cdot (\cos \theta - m \cdot 1_y)), \quad (6)$$

which is a form of applying HE on the CE loss, i.e., $\tilde{f}(x)$ includes FN and WN, and m indicates AM. Note that there is $\mathcal{L}_{CE}^0(\tilde{f}(x), y) = \mathcal{L}_{CE}(\tilde{f}(x), y)$ when the margin $m = 0$.

To highlight our main contributions in terms of methodology, we summarize the proposed formulas of AT in Table 1. We mainly consider three popular AT frameworks including **PGD-AT** (Madry et al., 2018), **ALP** (Kannan et al., 2018), and **TRADES** (Zhang et al., 2019b). The differences between our enhanced versions (with HE) from the original versions (without HE) are colorized in red. Note that we apply the HE mechanism both on the adversarial objective \mathcal{L}_A for constructing adversarial examples (the inner maximization problem), and the training objective \mathcal{L}_T for updating parameters (the outer minimization problem).

2.3. Related Work

In the face recognition domain, conventional pair-wise or triplet-wise metric learning was used to learn more generalizable feature space (Sun et al., 2014; Schroff et al., 2015). However, due to the high computational burden induced by metric learning, different variants of HE are presented and become popular on face recognition tasks (Wang et al., 2017a; Liu et al., 2017). As a reformulation of the metric learning, HE can efficiently learn more balanced and discriminative features with angular margins. In Appendix B.1, we extensively introduce the related work on combining metric learning with AT (Mao et al., 2019; Li et al., 2019; Zhang & Wang, 2019) and further present their bottlenecks.

3. Theoretical Analyses

In this section, we analyze the benefits induced by the mutual interaction between AT and HE. We consider the ℓ_p -

bounded threat model (Carlini et al., 2019), where $\mathbf{B}(x) = \{x' \mid \|x' - x\|_p \leq \epsilon\}$ and ϵ is the maximal perturbation.

3.1. Formalized First-order Adversary

Most of the adversarial attacks applied in AT belong to the family of first-order adversaries, due to the computational efficiency (Goodfellow et al., 2015; Madry et al., 2018). We first define the vector function \mathbb{U}_p as

$$\mathbb{U}_p(u) = \arg \max_{\|v\|_p \leq 1} u^\top v. \quad (7)$$

Let $\|\cdot\|_q$ be the dual norm of $\|\cdot\|_p$ with $\frac{1}{p} + \frac{1}{q} = 1$, we have $u^\top \mathbb{U}_p(u) = \|u\|_q$ by duality (Boyd & Vandenberghe, 2004). Specially, there are $\mathbb{U}_2(u) = \frac{u}{\|u\|_2}$ and $\mathbb{U}_\infty(u) = \text{sign}(u)$. If u is the gradient of a loss function \mathcal{L} , then $\mathbb{U}_p(u)$ is the direction of greatest increase of \mathcal{L} under the first-order Taylor expansion and the norm constraint, as stated below:

Lemma 1. (Proof in Appendix A.1) *Given a loss function \mathcal{L} and under the first-order Taylor expansion, the solution of*

$$\max_{\|x' - x\|_p \leq \epsilon} \mathcal{L}(x')$$

is $x^ = x + \epsilon \mathbb{U}_p(\nabla \mathcal{L}(x))$. Furthermore, there is $\mathcal{L}(x^*) = \mathcal{L}(x) + \epsilon \|\nabla \mathcal{L}(x)\|_q$, where $\|\cdot\|_q$ is the dual norm of $\|\cdot\|_p$.*

According to the formulations in Lemma 1, we can generally formalize the generation process of first-order adversaries under the ℓ_p -bounded threat model. For example, in the t -th iteration of the PGD attack with step size η (Madry et al., 2018), the adversarial example $x^{(t)}$ is updated as

$$x^{(t)} = x^{(t-1)} + \eta \mathbb{U}_p(\nabla \mathcal{L}(x^{(t-1)})), \quad (8)$$

where the increment of the loss is $\Delta \mathcal{L} = \mathcal{L}(x^{(t)}) - \mathcal{L}(x^{(t-1)}) = \eta \|\nabla \mathcal{L}(x^{(t-1)})\|_q$. We omit the clipping function and random initialization in PGD for convenience.

3.2. The Inner Maximization Problem in AT

As shown in Table 1, the adversarial objectives \mathcal{L}_A are usually the CE loss between two predictions (1_y as a ground-truth prediction). Thus, to optimize the inner maximization problem, we can expand the gradient of \mathcal{L}_A as below:

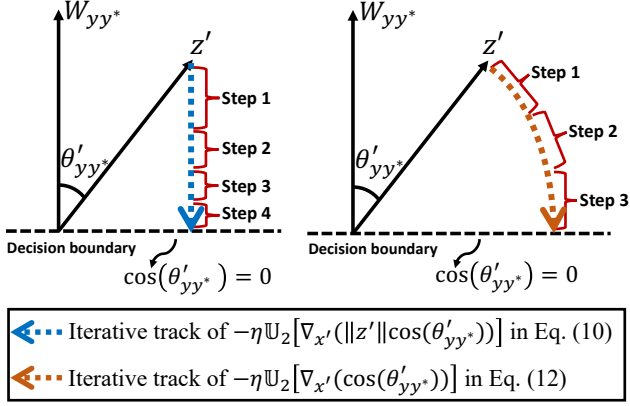


Figure 1. Intuitive illustration of taking fewer PGD iteration steps to move z' across the decision boundary when applying FN in \mathcal{L}_A .

Lemma 2. (Proof in Appendix A.2) By derivations, there is

$$\nabla_{x'} \mathcal{L}_{CE}(f(x'), f(x)) = - \sum_{i \neq j} f(x)_i f(x')_j \nabla_{x'} (W_{ij}^\top z'),$$

where $W_{ij} = W_i - W_j$, $z' = z(x'; \omega)$. When $f(x) = 1_y$, we have $\nabla_{x'} \mathcal{L}_{CE}(f(x'), y) = - \sum_{l \neq y} f(x')_l \nabla_{x'} (W_{yl}^\top z')$.

By substituting these equations into Eq. (8), we can obtain specific implementation to solve the inner maximization problem with PGD in different AT frameworks. To further simplify the expansions in Lemma 2, we let y^* be the predicted label on the finally crafted adversarial example x^* , where $y^* \neq y$. Then based on the empirical observations in previous work (Nguyen et al., 2015; Goodfellow et al., 2016), we are justified to assume that $f(x)_y$ is much larger than $f(x)_l$ for $l \neq y$, and $f(x')_{y^*}$ is much larger than $f(x')_l$ for $l \notin \{y, y^*\}$. Then according to Lemma 2, we have

$$\nabla_{x'} \mathcal{L}_{CE}(f(x'), f(x)) \approx -f(x)_y f(x')_{y^*} \nabla_{x'} (W_{yy^*}^\top z'). \quad (9)$$

By substituting Eq. (9) into Eq. (8), the update direction of each step in PGD becomes

$$\mathbb{U}_p [\nabla_{x'} \mathcal{L}_{CE}(f(x'), f(x))] \approx -\mathbb{U}_p [\nabla_{x'} (\|z'\| \cos(\theta'_{yy^*}))] \quad (10)$$

where $\theta'_{yy^*} = \angle(W_{yy^*}, z')$. Note that the approximation in Eq. (10) also holds when $f(x) = 1_y$.

3.3. Benefits from Feature Normalization

To investigate the effects of FN alone, we deactivate the WN operation in Eq. (5) and denote

$$\bar{f}(x) = \mathbb{S}(\mathbf{W}^\top \tilde{z}). \quad (11)$$

Then according to Eq. (10), we can obtain the update direction of PGD with FN applied as

$$\mathbb{U}_p [\nabla_{x'} \mathcal{L}_{CE}(\bar{f}(x'), \bar{f}(x))] \approx -\mathbb{U}_p [\nabla_{x'} (\cos(\theta'_{yy^*}))]. \quad (12)$$

Variation on $\|z'\|$ is ineffective. By comparing Eq. (10) and Eq. (12), we can find that applying FN in the adversarial objective \mathcal{L}_A eliminates the term of gradient on the feature norm $\|z'\|$. As shown in Fig. 1, the sufficient and necessary condition for x' is adversarial is that $\cos(\theta'_{yy^*}) < 0$, i.e., the feature z' moves across the decision boundary $\cos(\theta'_{yy^*}) = 0$. This means that the variation on the norm $\|z'\|$ will not change the model predictions (no bias term).

This difference is profitable because, in the adversarial attacks, we pursue minimizing the perturbation for elusiveness, while in AT we explore minimal necessary iteration steps for efficiency. Below we show that FN indeed renders it taking fewer iteration steps to craft adversarial examples.

Fewer iteration steps. As the common solver for the inner maximization problem in AT, the specific iterative updating process without or with FN in Eq. (8) are respectively

$$\begin{aligned} \mathbf{x}^{(t)} &= \mathbf{x}^{(t-1)} + \eta \mathbb{U}_p [\nabla_{\mathbf{x}} \mathcal{L}_{CE}(f(\mathbf{x}^{(t-1)}), f(x))]; \\ \mathbf{x}^{(t)} &= \mathbf{x}^{(t-1)} + \eta \mathbb{U}_p [\nabla_{\mathbf{x}} \mathcal{L}_{CE}(\bar{f}(\mathbf{x}^{(t-1)}), \bar{f}(x))]. \end{aligned} \quad (13)$$

where the colors blue and orange correspond to those shown in Fig. 1. Then under the approximation of Eq. (10) and Eq. (12), we can further derive from Lemma 1 that

$$\begin{aligned} \cos(\theta_{yy^*}^{(t)}) &> \cos(\theta_{yy^*}^{(t-1)}) - \eta \|\nabla_{\mathbf{x}} \cos(\theta_{yy^*}^{(t-1)})\|_q; \\ \cos(\theta_{yy^*}^{(t)}) &= \cos(\theta_{yy^*}^{(t-1)}) - \eta \|\nabla_{\mathbf{x}} \cos(\theta_{yy^*}^{(t-1)})\|_q. \end{aligned} \quad (14)$$

Here Eq. (14) shows that under the first-order Taylor expansion, applying FN in the adversarial objective \mathcal{L}_A can reduce $\cos(\theta'_{yy^*})$ to less than zero faster, i.e., with fewer iterations, no matter whether FN is also applied in the training objective \mathcal{L}_T . As intuitively illustrated in Fig. 1, the blue track (without FN) leads to the smallest perturbation but requires more iterations, while the orange track (with FN) moves to the decision boundary more directly with fewer iterations. This property is empirically verified in Fig. 4.

Better learning on hard examples. As to the benefits of applying FN in the training objective \mathcal{L}_T , we formally show that FN can promote learning on hard examples, as empirically observed in the previous work (Ranjan et al., 2017). By simple derivations (Goodfellow et al., 2016), we can obtain the gradients of the CE loss w.r.t. the model parameters ω and \mathbf{W} on a training pair (x, y) as

$$\begin{aligned} \nabla_{W_l} \mathcal{L}_{CE} &= \begin{cases} (f(x)_y - 1) \cdot z, & l = y, \\ f(x)_l \cdot z, & l \neq y, \end{cases} \\ \nabla_{\omega} \mathcal{L}_{CE} &= - \sum_{l \neq y} f(x)_l \cdot \|W_{yl}\| \nabla_{\omega} (\|z\| \cos(\theta_{yl})), \end{aligned} \quad (15)$$

where $\theta_{yl} = \angle(W_{yl}, z)$ and we omit the bias in Eq. (1) for simplicity. When FN is not applied, the model parameters ω is updated towards $-\nabla_{\omega} \mathcal{L}_{CE}$, which equals to

$$\sum_{l \neq y} f(x)_l \|W_{yl}\| (\cos(\theta_{yl}) \nabla_{\omega} \|z\| + \|z\| \nabla_{\omega} \cos(\theta_{yl})). \quad (16)$$

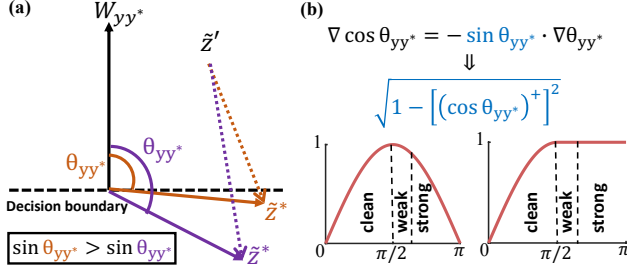


Figure 2. Demos: (a) Weak adversaries have higher weights on model update; (b) Modifications to better utilize strong adversaries.

According to Eq. (16), we can see that the training inputs with small $\nabla_{\omega} \|z\|$ or $\nabla_{\omega} \cos(\theta_{yl})$ contribute less in the direction of model updating, which are qualitatively defined as *hard examples*. This will cause the training process to devote non-effective efforts to increasing $\|z\|$ for easy examples, and consequently overlook the $\cos \theta_{yl}$ term for hard examples, which is critical for output predictions. Besides, as empirically shown in Fig. 6, the hard examples in AT are usually the crafted adversarial examples, which are those we actually expect the model to focus on in the AT procedure.

In comparison, when FN is applied, there are $\nabla_{\omega} \|\tilde{z}\| = 0$ and $\|\tilde{z}\| = s$, then ω is updated towards

$$\sum_{l \neq y} s \bar{f}(x)_l \cdot \|W_{yl}\| \nabla_{\omega} \cos(\theta_{yl}). \quad (17)$$

In this case, due to the bounded value range $[-1, 1]$ of cosine function, the easy examples will contribute less when they are well learned, i.e., have large $\cos(\theta_{yl})$, while the hard examples could later dominate the training. This causes a dynamic training procedure similar to curriculum learning (Bengio et al., 2009), which can improve generalization.

3.4. Benefits from Weight Normalization

In the AT procedures, the class biases in training could stem from the dataset itself, or the untargeted solver for the inner maximization problem, where the locations of the crafted adversarial features are uncontrolled. To understand how the class biases affect training, assuming that we perform the gradient descent on a data batch $\mathcal{D} = \{(x^k, y^k)\}_{k \in [N]}$. Then according to Eq. (15), we know that $\forall l \in [L]$, the softmax weight W_l is updated towards

$$-\nabla_{W_l} \mathcal{L}_{CE}(\mathcal{D}) = \sum_{x^k \in \mathcal{D}_l} z^k - \sum_{x^k \in \mathcal{D}} f(x^k)_l \cdot z^k, \quad (18)$$

where \mathcal{D}_l is the subset of \mathcal{D} with label l . We can see that the weight W_l will tend to have larger norm when there are more data or easy examples in class l , i.e., larger $|\mathcal{D}_l|$ or $\|z^k\|$ for $x^k \in \mathcal{D}_l$. Besides, if an input x in the batch is adversarial, then $f(x)_y$ is usually small and consequently z will have a large effect on the update of W_y . Since there is $W_{yy^*}^T z < 0$, W_y will be updated towards W_{yy^*} both in norm and direction, which causes repeatedly oscillation in AT.

When applying WN, the update of W_l will depend on the averaged feature direction of each class, and thus treat the weights more equally on unbalanced training data. WN can also alleviate the non-effective oscillation on the weight norm and speed up training (Salimans & Kingma, 2016). Besides, when FN and WN are both applied, the inner products $W^T z$ in the softmax layer will become scaled angular metric $s \cdot \cos \theta$, as shown in Eq. (5). Then we can naturally introduce AM to learn more discriminative and robust features (Elsayed et al., 2018; Yan et al., 2018).

3.5. Modifications to Better Utilize Strong Adversaries

In most of the AT procedures, each mini-batch of the crafted adversarial examples will only be used once in a single training step to update the model parameters (Madry et al., 2018). This means that unlike hard clean examples, hard adversarial examples would not have an chance to gradually dominate the training as introduced in Eq. (17). As illustrated in Fig. 2(a), since $\nabla_{\omega} \cos(\theta_{yy^*}) = -\sin(\theta_{yy^*}) \nabla_{\omega} \theta_{yy^*}$, the weak adversarial examples around the decision boundary with $\theta_{yy^*} \sim 90^\circ$ have higher weights $\sin(\theta_{yy^*})$. This makes the model tend to overlook the strong adversarial examples with large θ_{yy^*} , which contain abundant information.

To be better compatible with strong adversaries, it is straightforward to multiply the $\nabla_{\omega} \cos(\theta_{yl})$ term in Eq. (17) with, e.g., $\sqrt{1 - [(\cos \theta_{yl})^+]^2} / \sin(\theta_{yl})$ as shown in Fig. 2(b), where $(\cdot)^+ = \min(\cdot, 0)$. This modification assigns fairer weights to the adversarial examples with different severity, which prevents the models from overfitting to simple attacking patterns (Song et al., 2019). Another easy-to-implement way is to directly substitute $\mathbb{S}(s \cdot \cos \theta)$ in Eq. (5) with $\mathbb{S}(-s \cdot \theta)$, using the arccos operator. We name this form of embedding as modified HE (**m-HE**), as evaluated in Table 5.

4. Experiments

We experiment on the widely used CIFAR-10 (Krizhevsky & Hinton, 2009) and ImageNet (Deng et al., 2009) datasets.

CIFAR-10 setup. We follow the common setup adopted in previous work (Madry et al., 2018). We apply the wide residual network WRN-34-10 as the model architecture (Zagoruyko & Komodakis, 2016). For each AT framework, we set the maximal perturbation $\epsilon = 8/255$, the perturbation step size $\eta = 2/255$, and the number of iterations $K = 10$. We apply the momentum SGD (Qian, 1999) optimizer with the initial learning rate of 0.1, and train for 100 epochs. The learning rate decays with a factor of 0.1 at 75 and 90 epochs, respectively. The mini-batch size is 128. Besides, we set the regularization parameter $1/\lambda$ as 6 for TRADES, and set the adversarial logit pairing weight as 0.5 for ALP (Zhang et al., 2019b; Kannan et al., 2018). The scale $s = 15$ and the margin $m = 0.2$ in HE, where different s and m correspond to different trade-offs between the accuracy and robustness, as detailed in Appendix C.3.

Table 2. Classification accuracy (%) on **CIFAR-10** under the *white-box* threat model. The perturbation $\epsilon = 0.031$, step size $\eta = 0.003$.

Defense	Clean	PGD-20	PGD-500	MIM-20	FGSM	DeepFool	C&W- ℓ_∞
PGD-AT	86.75	53.97	51.63	55.08	59.70	57.26	84.00
PGD-AT + HE	86.19	59.36	57.59	60.19	63.77	61.56	84.07
ALP	87.18	52.29	50.13	53.35	58.99	59.40	84.96
ALP + HE	89.91	57.69	51.78	58.63	65.08	65.19	87.86
TRADES	84.62	56.48	54.84	57.14	61.02	60.70	81.13
TRADES + HE	84.88	62.02	60.75	62.71	65.69	60.48	81.44

 Table 3. Top-1 classification accuracy (%) on **ImageNet** under the *white-box* threat model. The notation * indicates the ablation study on the effect of each component in HE, where **HE=FN+WN+AM**.

Model	Method	Clean	PGD-10	PGD-50
ResNet-50	FreeAT	60.28	32.13	31.39
	FreeAT+WN *	60.39	32.53	31.68
	FreeAT+FN *	61.09	39.31	38.92
	FreeAT+FN+WN*	61.34	39.52	39.20
	FreeAT+HE	61.83	40.22	39.85
ResNet-152	FreeAT	65.20	36.97	35.87
	FreeAT+HE	65.41	43.24	42.60
WRN-50-2	FreeAT	64.18	36.24	35.38
	FreeAT+HE	65.28	43.83	43.47
WRN-101-2	FreeAT	66.15	39.35	38.23
	FreeAT+HE	66.37	45.35	45.04

ImageNet setup. AT on ImageNet usually requires tens or hundreds of GPU workers in parallel (Kurakin et al., 2017b; Xie et al., 2019). Due to the limited computation resource, we apply the framework of free adversarial training (**FreeAT**) in Shafahi et al. (2019), which has similar training objective as PGD-AT and can train a robust model using four GPU workers. We set the repeat times $m = 4$ in FreeAT. The maximal perturbation $\epsilon = 4/255$ with the step size $\eta = 1/255$. We train the model for 90 epochs with the initial learning rate of 0.1, and the mini-batch size is 256. The scale $s = 10$ and the margin $m = 0.2$ in HE.

4.1. Performance under White-box Attacks

Evaluation on CIFAR-10. We test the defenses under different attacks including FGSM (Goodfellow et al., 2015), PGD (Madry et al., 2018), MIM (Dong et al., 2018), Deepfool (Moosavi-Dezfooli et al., 2016), and C&W (ℓ_∞ version) (Carlini & Wagner, 2017a). We report the classification accuracy in Table 2 following the evaluation settings in Zhang et al. (2019b). We denote the iteration steps behind the attacking method, e.g., 10-step PGD as PGD-10. Besides, to verify that our strategy is generally compatible with previous work on accelerating AT, we combine HE with the one-step based FreeAT and fast adversarial training (**FastAT**) frameworks (Wong et al., 2020). In training, we run on a single GPU with the cyclic learning rate and mixed-precision arithmetic tricks (Coleman et al., 2017). We provide the accuracy and training time results in Table 5.

Besides, in Table 5 and Appendix C.4, we also evaluate embedding **m-HE** (introduced in Sec. 3.5) and find it more

 Figure 3. Classification accuracy (%) under the *black-box* transfer-based attacks on **CIFAR-10**. The substitute models are PGD-AT, ALP and TRADES separately. * indicates white-box cases.

		PGD-20			MIM-20		
		PGD-AT	ALP	TRADES	PGD-AT	ALP	TRADES
PGD-AT	53.93*	66.17	66.33	55.08*	66.02	66.45	
	66.30	52.26*	66.29	66.25	53.34*	66.51	
	65.83	66.12	56.48*	65.86	66.00	57.14*	
ALP	67.49	67.95	67.21	67.39	67.88	67.32	
	68.44	69.58	68.89	68.35	69.24	68.83	
	66.58	67.42	65.90	66.64	67.42	66.04	
TRADES	PGD-AT	ALP	TRADES	PGD-AT	ALP	TRADES	

effective than HE when combining with PGD-AT, FreeAT and Fast AT that exclusively train on adversarial examples.

Evaluation on ImageNet. Following the evaluation settings in Shafahi et al. (2019), we test under PGD-10 and PGD-50, as shown in Table 3. The models are trained using the architectures with different depth or width. When using ResNet-50 (He et al., 2016), we conduct extra ablation studies to investigate the effect of each operation in HE.

As indicated by the above results, when combining with the HE mechanism, the models trained under the PGD-AT, ALP, TRADES, FastAT, and FreeAT frameworks can consistently improve robustness and keep higher or comparable clean accuracy on different datasets and model architectures. Furthermore, the operations introduced by HE only increase negligible training time (less than 1%), even in the cases pursuing extremely fast training, as shown in Table 5. Our additional ablation studies imply that mapping the features on to the hypersphere by FN is the most critical operation in HE, while WN and AM facilitate the learned features to distribute more evenly and discriminatively.

4.2. Performance under Black-box Attacks

Transfer-based Black-box Attacks. Due to the adversarial transferability (Papernot et al., 2016a;b), the black-box adversaries can construct adversarial examples based on the substitute models and then feed these examples to evade the original models. In our experiments, we apply PGD-AT,

Table 4. Top-1 classification accuracy (%) on **CIFAR-10-C** and **ImageNet-C**. The models are trained on the original datasets CIFAR-10 and ImageNet, respectively. Here 'mCA' refers to the mean classification accuracy averaged on different corruptions and severity.

Defense	mCA	Noise			Blur				Weather				Digital			
		Gauss	Shot	Impulse	Defocus	Glass	Motion	Zoom	Snow	Frost	Fog	Bright	Contra	Elastic	Pixel	JPEG
CIFAR-10-C																
PGD-AT	77.23	81.65	82.88	74.52	81.84	79.69	77.62	80.88	81.32	77.95	61.70	84.05	44.55	80.79	84.76	84.35
PGD-AT + HE	77.29	81.54	82.47	76.14	81.84	79.45	78.17	80.87	80.77	77.98	62.45	83.67	45.11	80.69	84.16	84.10
ALP	77.73	82.29	83.41	74.87	81.94	80.31	78.23	80.97	81.74	79.26	61.51	84.88	45.86	80.91	85.09	84.68
ALP + HE	80.55	82.22	83.91	74.29	80.87	85.23	81.26	84.43	85.14	83.89	68.83	88.33	50.74	84.44	87.44	87.28
TRADES	75.36	79.22	80.37	72.90	79.84	77.72	76.34	78.66	79.52	76.94	59.68	82.06	43.80	78.53	82.65	82.31
TRADES+HE	75.78	78.88	80.21	73.81	80.55	77.61	77.26	79.62	79.23	76.53	61.39	82.33	45.04	79.29	82.50	82.40
ImageNet-C																
FreeAT	28.22	29.21	28.03	22.34	19.15	26.63	25.75	28.25	23.03	23.47	3.71	45.18	5.40	41.76	48.78	52.55
FreeAT+HE	30.04	27.63	25.75	19.86	21.16	29.28	28.08	30.76	26.62	28.35	5.34	49.88	7.03	44.72	51.17	55.05

Table 5. Validation of combining HE and m-HE with FastAT and FreeAT on **CIFAR-10**. We report the accuracy and training time.

Defense	Epo.	Clean (%)	PGD-50 (%)	Time (min)
FastAT	30	83.80	46.40	11.38
FastAT + HE	30	82.58	52.55	11.48
FastAT + m-HE	30	83.14	53.49	11.49
FreeAT	10	77.21	46.14	15.78
FreeAT + HE	10	76.85	50.98	15.87
FreeAT + m-HE	10	77.59	51.85	15.91

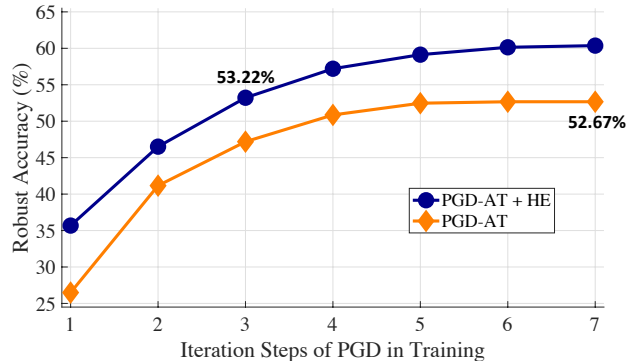


Figure 4. Robust accuracy (%) under PGD-20 on **CIFAR-10**. The models are trained by PGD-AT with different iteration steps.

ALP, and TRADES to train the substitute models, respectively. To generate adversarial perturbations, we employ the untargeted PGD-20 and MIM-20 attacks. In Fig. 3, we show the results of transfer-based attacks against the defense models trained without or with the HE mechanism.

Query-based Black-box Attacks. When the black-box adversaries are allowed to query the defenses many times before performing the attack, they can use more effective algorithms to break the models. Specifically, ZOO (Chen et al., 2017) proposes to estimate the gradient at each coordinate e_i as \hat{g}_i , with a small finite-difference σ . In experiments, we randomly select one sampled coordinate to perform one update with \hat{g}_i , and adopt the C&W optimization mechanism based on the estimated gradient. We set σ as 10^{-4} and max queries as 20,000. SPSA (Uesato et al., 2018) and NES (Ilyas et al., 2018) can make a full gradient

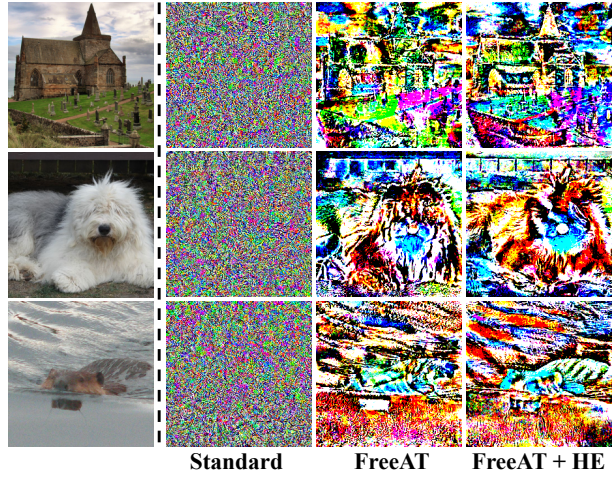


Figure 5. Visualizing the adversarial perturbations. The pixel values are re-scaled. We observe that the perturbations produced for the model trained with HE capture clearer and sharper profiles.

evaluation by drawing random samples and obtaining the corresponding loss values. NES randomly samples from a Gaussian distribution to acquire the direction vectors while SPSA samples from a Rademacher distribution. In experiments, we set the number of random samples q as 128 for every iteration and $\sigma = 0.001$. We show the robustness of different iterations against untargeted score-based ZOO, SPSA, and NES in Table 6, where detailed formulas of these attacks are provided in Appendix B.3.

As expected, these results show that embedding HE can generally provide promotion under the transfer-based and query-based black-box attacks, which verifies that our method can reliably improve robustness, rather than resulting in, e.g., gradient obfuscation (Athalye et al., 2018).

4.3. Performance under General-purpose Attacks

Although adversarially trained models could be more robust under the specified, e.g., ℓ_∞ -bounded threat model (Fawzi et al., 2016), they have been shown to be vulnerable to rotations (Engstrom et al., 2019), image corruptions (Gilmer

Table 6. Classification accuracy (%) under different *black-box* query-based attacks on **CIFAR-10**. The maximal perturbation is 8/255.

Method	Iterations	PGD-AT	PGD-AT + HE	ALP	ALP + HE	TRADES	TRADES + HE
ZOO	-	73.47	74.65	72.70	74.90	71.92	74.65
SPSA	20	73.64	73.66	73.11	74.45	72.12	72.36
	50	68.93	69.31	68.39	68.28	68.20	68.42
	80	65.67	65.97	65.14	63.89	65.32	65.62
	20	74.68	74.87	74.41	75.91	73.40	73.47
NES	50	71.22	71.48	70.81	71.11	70.29	70.53
	80	69.16	69.92	68.88	68.53	68.83	69.06

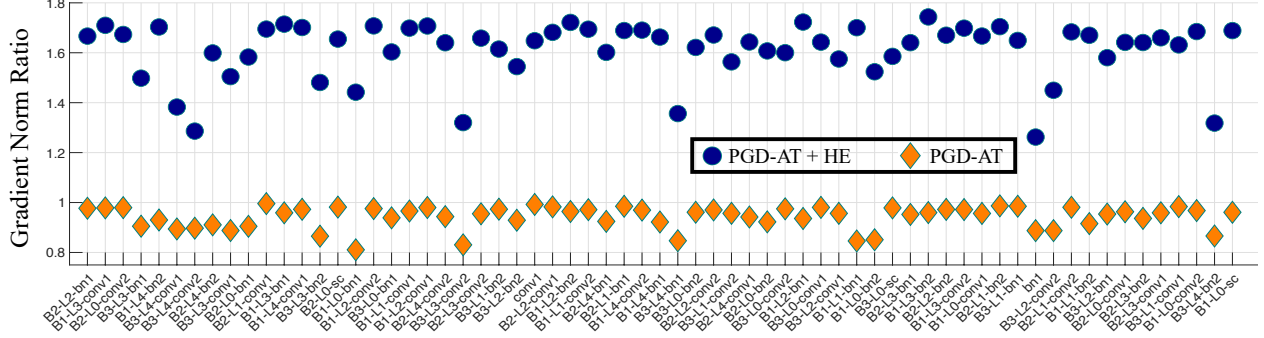


Figure 6. The ratios of $\mathbb{E}(\|\nabla_{\omega} \mathcal{L}(x^*)\|/\|\nabla_{\omega} \mathcal{L}(x)\|)$ w.r.t. different parameters ω , where x^* and x are the adversarial example and its clean counterpart. Higher ratio values indicate more attention on the adversarial examples in training, which can better utilize information and is critical for robust learning. 'B' refers to block, 'L' refers to layer, 'conv' refers to convolution, 'bn' refers to batch normalization.

et al., 2019) or affine attacks (Tramèr & Boneh, 2019). Therefore, to comprehensively evaluate the model robustness, we assess on the benchmarks with distributional shifts: CIFAR-10-C and ImageNet-C (Hendrycks & Dietterich, 2019). These two datasets include 15 types of common visual corruptions applied to the original clean datasets, where each kind of corruption has five different levels of severity.

As shown in Table 4, we report the classification accuracy under each corruption averaged on five levels of severity, where the models are WRN-34-10 trained on CIFAR-10 and ResNet-50 trained on ImageNet, respectively. Here we adopt accuracy as the metric to be consistent with other results in this paper, while the reported values can easily convert into the corruption error metric used in [Hendrycks & Dietterich \(2019\)](#). Besides higher mean accuracy, we can further find that our methods can lead to better robustness under a wide range of corruptions that are not seen in training, which indicates that embedding HE in AT can partly prevent the models from overfitting to certain attacking pattern.

4.4. More Empirical Analyses

To further understand and visualize the properties of the proposed methods, we conduct more empirical trials to reflect the formal analyses in Sec. 3. We first investigate the relation between the robust accuracy and the iteration steps of PGD in training for PGD-AT. As shown in Fig. 4, we separately use PGD-1 to PGD-7 to generate adversarial examples in training, then we evaluate the trained models under the PGD-20 attack. We can see that our method requires fewer iterations of PGD to achieve certain robust accuracy. For

example, applying 3-step PGD in PGD-AT+HE is more robust than applying 7-step PGD in PGD-AT, which largely reduces the necessary computation (Wang et al., 2019).

Furthermore, previous studies observe that the adversarial examples against robust models exhibit salient data characteristics (Tsipras et al., 2019; Tao et al., 2018; Zhang & Zhu, 2019; Ilyas et al., 2019). So we provide a visualization of the untargeted perturbations on ImageNet, as shown in Fig. 5. We compare the standardly trained model and two robust models trained by FreeAT and FreeAT+HE, respectively. We can observe that the adversarial perturbations produced for our method have sharper profiles and more concrete details, which are better aligned with human perception.

In Fig. 6, we calculate the norm ratios of the loss gradient on the adversarial example to it on the clean example w.r.t. different parameters. The model is trained for 70 epochs on CIFAR-10 using PGD-AT. The results verify the analysis in Sec.3 that our method can prompt the training procedure to assign larger gradients on learning the constructed adversarial examples, which would benefit robust learning.

5. Conclusion

In this paper, we propose to embed the HE operations into AT to enhance the performance of the adversarially trained models. We analyze the intriguing benefits induced by the interaction between AT and HE, as well as presenting potential variants like m-HE to adapt to different training contexts. In our experiments, we comprehensively verify that HE is consistently conducive to different AT frameworks, with little extra computation and simple code implementation.

References

Alayrac, Jean-Baptiste, Uesato, Jonathan, Huang, Po-Sen, Fawzi, Alhussein, Stanforth, Robert, and Kohli, Pushmeet. Are labels required for improving adversarial robustness? In *Advances in Neural Information Processing Systems (NeurIPS)*, pp. 12192–12202, 2019.

Athalye, Anish, Carlini, Nicholas, and Wagner, David. Obfuscated gradients give a false sense of security: Circumventing defenses to adversarial examples. In *International Conference on Machine Learning (ICML)*, 2018.

Bengio, Yoshua, Louradour, Jérôme, Collobert, Ronan, and Weston, Jason. Curriculum learning. In *International Conference on Machine Learning (ICML)*, pp. 41–48. ACM, 2009.

Biggio, Battista, Corona, Igino, Maiorca, Davide, Nelson, Blaine, Šrndić, Nedim, Laskov, Pavel, Giacinto, Giorgio, and Roli, Fabio. Evasion attacks against machine learning at test time. In *Joint European conference on machine learning and knowledge discovery in databases*, pp. 387–402. Springer, 2013.

Boyd, Stephen and Vandenberghe, Lieven. *Convex optimization*. Cambridge university press, 2004.

Brendel, Wieland, Rauber, Jonas, Kurakin, Alexey, Papernot, Nicolas, Veliqi, Behar, Mohanty, Sharada P, Laurent, Florian, Salathé, Marcel, Bethge, Matthias, Yu, Yaodong, et al. Adversarial vision challenge. In *The NeurIPS'18 Competition*, pp. 129–153. Springer, 2020.

Carlini, Nicholas and Wagner, David. Towards evaluating the robustness of neural networks. In *IEEE Symposium on Security and Privacy (S&P)*, 2017a.

Carlini, Nicholas and Wagner, David. Adversarial examples are not easily detected: Bypassing ten detection methods. In *ACM Workshop on Artificial Intelligence and Security (AISec)*, 2017b.

Carlini, Nicholas, Athalye, Anish, Papernot, Nicolas, Brendel, Wieland, Rauber, Jonas, Tsipras, Dimitris, Goodfellow, Ian, Madry, Aleksander, and Kurakin, Alexey. On evaluating adversarial robustness. *arXiv preprint arXiv:1902.06705*, 2019.

Carmon, Yair, Raghunathan, Aditi, Schmidt, Ludwig, Liang, Percy, and Duchi, John C. Unlabeled data improves adversarial robustness. In *Advances in Neural Information Processing Systems (NeurIPS)*, 2019.

Chen, Pin-Yu, Zhang, Huan, Sharma, Yash, Yi, Jinfeng, and Hsieh, Cho-Jui. Zoo: Zeroth order optimization based black-box attacks to deep neural networks without training substitute models. In *Proceedings of the 10th ACM Workshop on Artificial Intelligence and Security (AISec)*, ACM, 2017.

Coleman, Cody, Narayanan, Deepak, Kang, Daniel, Zhao, Tian, Zhang, Jian, Nardi, Luigi, Bailis, Peter, Olukotun, Kunle, Ré, Chris, and Zaharia, Matei. Dawnbench: An end-to-end deep learning benchmark and competition. *Training*, 100(101):102, 2017.

Deng, Jia, Dong, Wei, Socher, Richard, Li, Li-Jia, Li, Kai, and Fei-Fei, Li. Imagenet: A large-scale hierarchical image database. In *Proceedings of the IEEE Conference on Computer Vision and Pattern Recognition (CVPR)*, 2009.

Deng, Jiankang, Guo, Jia, Xue, Niannan, and Zafeiriou, Stefanos. Arcface: Additive angular margin loss for deep face recognition. In *Proceedings of the IEEE Conference on Computer Vision and Pattern Recognition (CVPR)*, 2019.

Dong, Yinpeng, Liao, Fangzhou, Pang, Tianyu, Su, Hang, Zhu, Jun, Hu, Xiaolin, and Li, Jianguo. Boosting adversarial attacks with momentum. In *Proceedings of the IEEE Conference on Computer Vision and Pattern Recognition (CVPR)*, 2018.

Dong, Yinpeng, Fu, Qi-An, Yang, Xiao, Pang, Tianyu, Su, Hang, Xiao, Zihao, and Zhu, Jun. Benchmarking adversarial robustness. *arXiv preprint arXiv:1912.11852*, 2019.

Elsayed, Gamaleldin, Krishnan, Dilip, Mobahi, Hossein, Regan, Kevin, and Bengio, Samy. Large margin deep networks for classification. In *Advances in neural information processing systems (NeurIPS)*, pp. 842–852, 2018.

Engstrom, Logan, Ilyas, Andrew, and Athalye, Anish. Evaluating and understanding the robustness of adversarial logit pairing. *arXiv preprint arXiv:1807.10272*, 2018.

Engstrom, Logan, Tran, Brandon, Tsipras, Dimitris, Schmidt, Ludwig, and Madry, Aleksander. A rotation and a translation suffice: Fooling cnns with simple transformations. In *International Conference on Machine Learning (ICML)*, 2019.

Fawzi, Alhussein, Moosavi-Dezfooli, Seyed-Mohsen, and Frossard, Pascal. Robustness of classifiers: from adversarial to random noise. In *Advances in Neural Information Processing Systems (NeurIPS)*, pp. 1632–1640, 2016.

Gilmer, Justin, Ford, Nicolas, Carlini, Nicolas, and Cubuk, Ekin. Adversarial examples are a natural consequence of test error in noise. In *International Conference on Machine Learning (ICML)*, 2019.

Goodfellow, Ian, Bengio, Yoshua, and Courville, Aaron. *Deep Learning*. MIT Press, 2016. <http://www.deeplearningbook.org>.

Goodfellow, Ian J, Shlens, Jonathon, and Szegedy, Christian. Explaining and harnessing adversarial examples. In *International Conference on Learning Representations (ICLR)*, 2015.

Gowal, Sven, Uesato, Jonathan, Qin, Chongli, Huang, Po-Sen, Mann, Timothy, and Kohli, Pushmeet. An alternative surrogate loss for pgd-based adversarial testing. *arXiv preprint arXiv:1910.09338*, 2019.

Guo, Yandong and Zhang, Lei. One-shot face recognition by promoting underrepresented classes. *arXiv preprint arXiv:1707.05574*, 2017.

He, Kaiming, Zhang, Xiangyu, Ren, Shaoqing, and Sun, Jian. Identity mappings in deep residual networks. In *European Conference on Computer Vision (ECCV)*, pp. 630–645. Springer, 2016.

Hendrycks, Dan and Dietterich, Thomas. Benchmarking neural network robustness to common corruptions and perturbations. In *International Conference on Learning Representations (ICLR)*, 2019.

Hendrycks, Dan, Lee, Kimin, and Mazeika, Mantas. Using pre-training can improve model robustness and uncertainty. In *International Conference on Machine Learning (ICML)*, 2019.

Hoffer, Elad and Ailon, Nir. Deep metric learning using triplet network. In *International Workshop on Similarity-Based Pattern Recognition*, pp. 84–92. Springer, 2015.

Ilyas, Andrew, Engstrom, Logan, Athalye, Anish, and Lin, Jessy. Black-box adversarial attacks with limited queries and information. In *International Conference on Machine Learning (ICML)*, 2018.

Ilyas, Andrew, Santurkar, Shibani, Tsipras, Dimitris, Engstrom, Logan, Anish Athalye, Tran, Brandon, and Madry, Aleksander. Adversarial examples are not bugs, they are features. In *Advances in Neural Information Processing Systems (NeurIPS)*, 2019.

Kannan, Harini, Kurakin, Alexey, and Goodfellow, Ian. Adversarial logit pairing. *arXiv preprint arXiv:1803.06373*, 2018.

Kingma, Diederik and Ba, Jimmy. Adam: A method for stochastic optimization. In *International Conference on Learning Representations (ICLR)*, 2015.

Krizhevsky, Alex and Hinton, Geoffrey. Learning multiple layers of features from tiny images. Technical report, Citeseer, 2009.

Kurakin, Alexey, Goodfellow, Ian, and Bengio, Samy. Adversarial examples in the physical world. In *The International Conference on Learning Representations (ICLR) Workshops*, 2017a.

Kurakin, Alexey, Goodfellow, Ian, and Bengio, Samy. Adversarial machine learning at scale. In *International Conference on Learning Representations (ICLR)*, 2017b.

Kurakin, Alexey, Goodfellow, Ian, Bengio, Samy, Dong, Yinpeng, Liao, Fangzhou, Liang, Ming, Pang, Tianyu, Zhu, Jun, Hu, Xiaolin, Xie, Cihang, et al. Adversarial attacks and defences competition. *arXiv preprint arXiv:1804.00097*, 2018.

Li, Pengcheng, Yi, Jinfeng, Zhou, Bowen, and Zhang, Lijun. Improving the robustness of deep neural networks via adversarial training with triplet loss. *arXiv preprint arXiv:1905.11713*, 2019.

Liu, Weiyang, Wen, Yandong, Yu, Zhiding, and Yang, Meng. Large-margin softmax loss for convolutional neural networks. In *International Conference on Machine Learning (ICML)*, 2016.

Liu, Weiyang, Wen, Yandong, Yu, Zhiding, Li, Ming, Raj, Bhiksha, and Song, Le. Sphereface: Deep hypersphere embedding for face recognition. In *Proceedings of the IEEE conference on computer vision and pattern recognition (CVPR)*, pp. 212–220, 2017.

Madry, Aleksander, Makelov, Aleksandar, Schmidt, Ludwig, Tsipras, Dimitris, and Vladu, Adrian. Towards deep learning models resistant to adversarial attacks. In *International Conference on Learning Representations (ICLR)*, 2018.

Mao, Chengzhi, Zhong, Ziyuan, Yang, Junfeng, Vondrick, Carl, and Ray, Baishakhi. Metric learning for adversarial robustness. In *Advances in Neural Information Processing Systems (NeurIPS)*, pp. 478–489, 2019.

Moosavi-Dezfooli, Seyed-Mohsen, Fawzi, Alhussein, and Frossard, Pascal. Deepfool: a simple and accurate method to fool deep neural networks. In *Proceedings of the IEEE Conference on Computer Vision and Pattern Recognition (CVPR)*, pp. 2574–2582, 2016.

Nguyen, Anh, Yosinski, Jason, and Clune, Jeff. Deep neural networks are easily fooled: High confidence predictions for unrecognizable images. In *Proceedings of the IEEE Conference on Computer Vision and Pattern Recognition (CVPR)*, pp. 427–436, 2015.

Pang, Tianyu, Du, Chao, and Zhu, Jun. Max-mahalanobis linear discriminant analysis networks. In *International Conference on Machine Learning (ICML)*, 2018.

Pang, Tianyu, Xu, Kun, Du, Chao, Chen, Ning, and Zhu, Jun. Improving adversarial robustness via promoting ensemble diversity. In *International Conference on Machine Learning (ICML)*, 2019.

Pang, Tianyu, Xu, Kun, Dong, Yinpeng, Du, Chao, Chen, Ning, and Zhu, Jun. Rethinking softmax cross-entropy loss for adversarial robustness. In *International Conference on Learning Representations (ICLR)*, 2020.

Papernot, Nicolas, McDaniel, Patrick, and Goodfellow, Ian. Transferability in machine learning: from phenomena to black-box attacks using adversarial samples. *arXiv preprint arXiv:1605.07277*, 2016a.

Papernot, Nicolas, McDaniel, Patrick, Goodfellow, Ian, Jha, Somesh, Celik, Z Berkay, and Swami, Ananthram. Practical black-box attacks against deep learning systems using adversarial examples. *arXiv preprint arXiv:1602.02697*, 2016b.

Parkhi, Omkar M, Vedaldi, Andrea, Zisserman, Andrew, et al. Deep face recognition. In *The British Machine Vision Conference (BMVC)*, 2015.

Paszke, Adam, Gross, Sam, Massa, Francisco, Lerer, Adam, Bradbury, James, Chanan, Gregory, Killeen, Trevor, Lin, Zeming, Gimelshein, Natalia, Antiga, Luca, et al. Pytorch: An imperative style, high-performance deep learning library. In *Advances in Neural Information Processing Systems (NeurIPS)*, pp. 8024–8035, 2019.

Qian, Ning. On the momentum term in gradient descent learning algorithms. *Neural networks*, 12(1):145–151, 1999.

Ranjan, Rajeev, Castillo, Carlos D, and Chellappa, Rama. L2-constrained softmax loss for discriminative face verification. *arXiv preprint arXiv:1703.09507*, 2017.

Salimans, Tim and Kingma, Durk P. Weight normalization: A simple reparameterization to accelerate training of deep neural networks. In *Advances in Neural Information Processing Systems (NeurIPS)*, pp. 901–909, 2016.

Schroff, Florian, Kalenichenko, Dmitry, and Philbin, James. Facenet: A unified embedding for face recognition and clustering. In *Proceedings of the IEEE Conference on Computer Vision and Pattern Recognition (CVPR)*, pp. 815–823, 2015.

Shafahi, Ali, Najibi, Mahyar, Ghiasi, Amin, Xu, Zheng, Dickerson, John, Studer, Christoph, Davis, Larry S, Taylor, Gavin, and Goldstein, Tom. Adversarial training for free! In *Advances in Neural Information Processing Systems (NeurIPS)*, 2019.

Song, Chuanbiao, He, Kun, Wang, Liwei, and Hopcroft, John E. Improving the generalization of adversarial training with domain adaptation. In *International Conference on Learning Representations (ICLR)*, 2019.

Sun, Yi, Chen, Yuheng, Wang, Xiaogang, and Tang, Xiaoou. Deep learning face representation by joint identification-verification. In *Advances in neural information processing systems (NeurIPS)*, pp. 1988–1996, 2014.

Szegedy, Christian, Zaremba, Wojciech, Sutskever, Ilya, Bruna, Joan, Erhan, Dumitru, Goodfellow, Ian, and Fergus, Rob. Intriguing properties of neural networks. In *International Conference on Learning Representations (ICLR)*, 2014.

Tao, Guanhong, Ma, Shiqing, Liu, Yingqi, and Zhang, Xiangyu. Attacks meet interpretability: Attribute-steered detection of adversarial samples. In *Advances in Neural Information Processing Systems (NeurIPS)*, pp. 7717–7728, 2018.

Tramèr, Florian and Boneh, Dan. Adversarial training and robustness for multiple perturbations. In *Advances in Neural Information Processing Systems (NeurIPS)*, pp. 5858–5868, 2019.

Tramèr, Florian, Kurakin, Alexey, Papernot, Nicolas, Boneh, Dan, and McDaniel, Patrick. Ensemble adversarial training: Attacks and defenses. In *International Conference on Learning Representations (ICLR)*, 2018.

Tsipras, Dimitris, Santurkar, Shibani, Engstrom, Logan, Turner, Alexander, and Madry, Aleksander. Robustness may be at odds with accuracy. In *International Conference on Learning Representations (ICLR)*, 2019.

Uesato, Jonathan, O’Donoghue, Brendan, Oord, Aaron van den, and Kohli, Pushmeet. Adversarial risk and the dangers of evaluating against weak attacks. In *International Conference on Machine Learning (ICML)*, 2018.

Wang, Feng, Xiang, Xiang, Cheng, Jian, and Yuille, Alan Loddon. Normface: 1 2 hypersphere embedding for face verification. In *Proceedings of the 25th ACM international conference on Multimedia (ACM MM)*, pp. 1041–1049. ACM, 2017a.

Wang, Hao, Wang, Yitong, Zhou, Zheng, Ji, Xing, Gong, Dihong, Zhou, Jingchao, Li, Zhifeng, and Liu, Wei. Cosface: Large margin cosine loss for deep face recognition. In *Proceedings of the IEEE Conference on Computer Vision and Pattern Recognition (CVPR)*, pp. 5265–5274, 2018.

Wang, Jian, Zhou, Feng, Wen, Shilei, Liu, Xiao, and Lin, Yuanqing. Deep metric learning with angular loss. In *Proceedings of the IEEE International Conference on Computer Vision (ICCV)*, pp. 2593–2601, 2017b.

Wang, Yisen, Ma, Xingjun, Bailey, James, Yi, Jinfeng, Zhou, Bowen, and Gu, Quanquan. On the convergence and robustness of adversarial training. In *International Conference on Machine Learning (ICML)*, pp. 6586–6595, 2019.

Wong, Eric, Rice, Leslie, and Kolter, J. Zico. Fast is better than free: Revisiting adversarial training. In *International Conference on Learning Representations (ICLR)*, 2020.

Wu, Tong, Tong, Liang, and Vorobeychik, Yevgeniy. Defending against physically realizable attacks on image classification. In *International Conference on Learning Representations (ICLR)*, 2020.

Wu, Zhirong, Xiong, Yuanjun, Yu, Stella X, and Lin, Dahua. Unsupervised feature learning via non-parametric instance discrimination. In *Proceedings of the IEEE Conference on Computer Vision and Pattern Recognition (CVPR)*, pp. 3733–3742, 2018.

Xie, Cihang, Wu, Yuxin, van der Maaten, Laurens, Yuille, Alan, and He, Kaiming. Feature denoising for improving adversarial robustness. In *Proceedings of the IEEE Conference on Computer Vision and Pattern Recognition (CVPR)*, 2019.

Yan, Ziang, Guo, Yiwen, and Zhang, Changshui. Deep defense: Training dnns with improved adversarial robustness. In *Advances in Neural Information Processing Systems (NeurIPS)*, pp. 419–428, 2018.

Zagoruyko, Sergey and Komodakis, Nikos. Wide residual networks. In *The British Machine Vision Conference (BMVC)*, 2016.

Zhang, Dinghuai, Zhang, Tianyuan, Lu, Yiping, Zhu, Zhanxing, and Dong, Bin. You only propagate once: Accelerating adversarial training via maximal principle. In *Advances in Neural Information Processing Systems (NeurIPS)*, 2019a.

Zhang, Haichao and Wang, Jianyu. Defense against adversarial attacks using feature scattering-based adversarial training. In *Advances in Neural Information Processing Systems (NeurIPS)*, pp. 1829–1839, 2019.

Zhang, Hongyang, Yu, Yaodong, Jiao, Jiantao, Xing, Eric P, Ghaoui, Laurent El, and Jordan, Michael I. Theoretically principled trade-off between robustness and accuracy. In *International Conference on Machine Learning (ICML)*, 2019b.

Zhang, Richard. Making convolutional networks shift-invariant again. In *International Conference on Machine Learning (ICML)*, 2019.

Zhang, Tianyuan and Zhu, Zhanxing. Interpreting adversarially trained convolutional neural networks. In *International Conference on Machine Learning (ICML)*, 2019.

A. Proofs

A.1. Proof of Lemma 1

Lemma 1. *Given a loss function \mathcal{L} and under the first-order Taylor expansion, the solution of*

$$\max_{\|x' - x\|_p \leq \epsilon} \mathcal{L}(x')$$

is $x^* = x + \epsilon \mathbb{U}_p(\nabla \mathcal{L}(x))$. Furthermore, there is $\mathcal{L}(x^*) = \mathcal{L}(x) + \epsilon \|\nabla \mathcal{L}(x)\|_q$, where $\|\cdot\|_q$ is the dual norm of $\|\cdot\|_p$.

Proof. We denote $x' = x + \epsilon v$, where $\|v\|_p \leq 1$. Then we know that $\|x' - x\|_p \leq \epsilon$. Under the first-order Taylor expansion, there is

$$\begin{aligned} \max_{\|x' - x\|_p \leq \epsilon} \mathcal{L}(x') &= \max_{\|v\|_p \leq 1} [\mathcal{L}(x) + \epsilon v^\top \nabla \mathcal{L}(x)] \\ &= \mathcal{L}(x) + \epsilon \max_{\|v\|_p \leq 1} v^\top \nabla \mathcal{L}(x). \end{aligned}$$

According to the definition of the dual norm (Boyd & Vandenberghe, 2004), there is $\max_{\|v\|_p \leq 1} v^\top \nabla \mathcal{L}(x) = \|\nabla \mathcal{L}(x)\|_q$, where $\|\cdot\|_q$ is the dual norm of $\|\cdot\|_p$. Thus we prove that $\mathcal{L}(x^*) = \mathcal{L}(x) + \epsilon \|\nabla \mathcal{L}(x)\|_q$ and $x^* = x + \epsilon \mathbb{U}_p(\nabla \mathcal{L}(x))$. \square

A.2. Proof of Lemma 2

Lemma 2. *By derivations, there is*

$$\nabla_{x'} \mathcal{L}_{CE}(f(x'), f(x)) = - \sum_{i \neq j} f(x)_i f(x')_j \nabla_{x'} (W_{ij}^\top z'),$$

where $W_{ij} = W_i - W_j$, $z' = z(x'; \omega)$. When $f(x) = 1_y$, we have $\nabla_{x'} \mathcal{L}_{CE}(f(x'), y) = - \sum_{l \neq y} f(x')_l \nabla_{x'} (W_{yl}^\top z')$.

Proof. By derivations, there is

$$\begin{aligned} -\nabla_{x'} \mathcal{L}_{CE}(f(x'), f(x)) &= \nabla_{x'} (f(x)^\top \log f(x')) \\ &= \sum_{i \in [L]} f(x)_i \nabla_{x'} \log(f(x')_i) \\ &= \sum_{i \in [L]} f(x)_i \nabla_{x'} \log \left(\frac{\exp(W_i^\top z')}{\sum_{j \in [L]} \exp(W_j^\top z')} \right) \\ &= \sum_{i \in [L]} f(x)_i \nabla_{x'} \left(W_i^\top z' - \log \left(\sum_{j \in [L]} \exp(W_j^\top z') \right) \right) \\ &= \sum_{i \in [L]} f(x)_i \left(\nabla_{x'} (W_i^\top z') - \sum_{j \in [L]} f(x')_j \nabla_{x'} (W_j^\top z') \right) \\ &= \sum_{i \in [L]} f(x)_i \left(\sum_{j \neq i} f(x')_j \nabla_{x'} (W_{ij}^\top z') \right) \\ &= \sum_{i \neq j} f(x)_i f(x')_j \nabla_{x'} (W_{ij}^\top z'). \end{aligned}$$

Specially, when $f(x) = 1_y$, we can obtain based on the above formulas that

$$\nabla_{x'} \mathcal{L}_{CE}(f(x'), y) = - \sum_{l \neq y} f(x')_l \nabla_{x'} (W_{yl}^\top z').$$

\square

B. More Preliminary Knowledge

In this section, we introduce more details on the preliminary knowledge concerned on the previous related work.

B.1. Metric Learning + Adversarial Training

Previous work finds that the adversarial attack would cause the internal representation to shift closer to the false class (Mao et al., 2019; Li et al., 2019). Based on this observation, they propose to introduce an extra triplet loss term in the training objective to capture the stable metric space representation, formulated as

$$\begin{aligned} &\mathcal{L}_{trip}(z(x^*), z(x_p), z(x_n)) \\ &= [D(z(x^*), z(x_p)) - D(z(x^*), z(x_n)) + \alpha]^+, \end{aligned} \quad (19)$$

where $\alpha > 0$ is a hyperparameter for margin, x^* (anchor example) is an adversarial counterpart based on the clean input x , x_p (positive example) is a clean image from the same class of x ; x_n (negative example) is a clean image from a different class. Here $D(u, v)$ is a distance function. Mao et al. (2019) employ an angular distance as $D(u, v) = 1 - \cos \angle(u, v)$; Li et al. (2019) apply the ℓ_∞ distance as $D(u, v) = \|u - v\|_\infty$. In the implementation, these methods apply some heuristic strategies to sample triplets, in order to alleviate high computation overhead. For example, Mao et al. (2019) select the closest sample in a mini-batch as an approximation to the semi-hard negative example. However, the optimization on sampled triplets is still computationally expensive and could introduce class biases on unbalanced datasets (Hoffer & Ailon, 2015).

Zhang & Wang (2019) apply a feature-scatter solver for the inner maximization problem of AT, which is different from PGD. Instead of crafting each adversarial example based on its clean counterpart, the feature-scatter solver generate the adversarial examples in batch to utilize inter-sample interactions, via maximizing the optimal transport (OT) distance between the clean and adversarial empirical distributions. In the implementation, they use practical OT-solvers to calculate the OT distance and maximize it w.r.t. the adversarial examples. However, the calculation of the OT distance will increase the computational burden for the AT procedure. Besides, the feature-scatter solver also leads to potential threats for the trained models to be evaded by adaptive attacks, e.g., feature attacks, as discussed before²³.

²<https://github.com/Line290/FeatureAttack>

³<https://openreview.net/forum?id=Syejj0NYvr¬eId=rkeBhuBMjS>

B.2. Adversarial Threat Models

Now we introduce different threat models in the adversarial setting following the suggestions in Carlini et al. (2019). Specifically, a threat model includes a set of assumptions about the adversary’s goals, capabilities, and knowledge.

Adversary’s goals could be simply fooling the classifiers to misclassify, which is referred to as *untargeted mode*. On the other hand, the goals can be more aggressive to make the model misclassify from a source class into a target class, which is referred to as *targeted mode*.

Adversary’s capabilities describe the constraints imposed on the attackers. For the ℓ_p bounded threat models, adversarial examples require the perturbation δ to be bounded by a preset threshold ϵ under ℓ_p -norm, i.e., $\|\delta\|_p \leq \epsilon$.

Adversary’s knowledge tells what knowledge the adversary is assumed to own. Typically, there are four settings when evaluating a defense method:

- *Oblivious adversaries* are not aware of the existence of the defense D and generate adversarial examples based on the unsecured classification model F (Carlini & Wagner, 2017b).
- *White-box adversaries* know the scheme and parameters of D , and can design adaptive methods to attack both the model F and the defense D simultaneously (Athalye et al., 2018).
- *Black-box adversaries* have no access to the parameters of the defense D or the model F with varying degrees of black-box access (Dong et al., 2018).
- *General-purpose adversaries* apply general transformations or corruptions on the images, which are related to traditional research topics on the input invariances (Hendrycks et al., 2019; Zhang, 2019).

B.3. Adversarial Attacks

Below we show the details of the attack methods that we test on in our experiments. For clarity, we only introduce the untargeted attacks. The descriptions below mainly adopt from Dong et al. (2019).

FGSM (Goodfellow et al., 2015) generates an untargeted adversarial example under the ℓ_∞ norm as

$$\mathbf{x}^{adv} = \mathbf{x} + \epsilon \cdot \text{sign}(\nabla_{\mathbf{x}} \mathcal{L}_{CE}(\mathbf{x}, y)). \quad (20)$$

BIM (Kurakin et al., 2017a) extends FGSM by iteratively taking multiple small gradient updates as

$$\mathbf{x}_{t+1}^{adv} = \text{clip}_{\mathbf{x}, \epsilon}(\mathbf{x}_t^{adv} + \eta \cdot \text{sign}(\nabla_{\mathbf{x}} \mathcal{L}_{CE}(\mathbf{x}_t^{adv}, y))), \quad (21)$$

where $\text{clip}_{\mathbf{x}, \epsilon}$ projects the adversarial example to satisfy the ℓ_∞ constraint and η is the step size.

PGD (Madry et al., 2018) is similar to BIM except that the initial point \mathbf{x}_0^{adv} is uniformly sampled from the neighborhood around the clean input x , which can cover wider diversity of the adversarial space (Wong et al., 2020).

MIM (Dong et al., 2018) integrates a momentum term into BIM with the decay factor $\mu = 1.0$ as

$$\mathbf{g}_{t+1} = \mu \cdot \mathbf{g}_t + \frac{\nabla_{\mathbf{x}} \mathcal{L}_{CE}(\mathbf{x}_t^{adv}, y)}{\|\nabla_{\mathbf{x}} \mathcal{L}_{CE}(\mathbf{x}_t^{adv}, y)\|_1}, \quad (22)$$

where the adversarial examples are updated by

$$\mathbf{x}_{t+1}^{adv} = \text{clip}_{\mathbf{x}, \epsilon}(\mathbf{x}_t^{adv} + \alpha \cdot \text{sign}(\mathbf{g}_{t+1})). \quad (23)$$

MIM has good performance as a transfer-based attack, which won the NeurIPS 2017 Adversarial Competition (Kurakin et al., 2018). We set the step size η and the number of iterations identical to those in BIM.

DeepFool (Moosavi-Dezfooli et al., 2016) is also an iterative attack method, which generates an adversarial example on the decision boundary of a classifier with the minimum perturbation. We set the maximum number of iterations as 100 in DeepFool, and it will early stop when the solution at an intermediate iteration is already adversarial.

C&W (Carlini & Wagner, 2017a) is a powerful optimization-based attack method, which generates an ℓ_2 adversarial example \mathbf{x}^{adv} by solving

$$\begin{aligned} \arg \min_{\mathbf{x}'} \{ & c \cdot \max(Z(\mathbf{x}'))_y - \max_{i \neq y} Z(\mathbf{x}')_i, 0 \\ & + \|\mathbf{x}' - \mathbf{x}\|_2^2 \}, \end{aligned} \quad (24)$$

where $Z(\mathbf{x}')$ is the logit output of the classifier and c is a constant. This optimization problem is solved by an Adam (Kingma & Ba, 2015) optimizer. c is found by binary search. The C&W attack can also be applied under the ℓ_∞ threat model with the adversarial loss function $\max(Z(\mathbf{x}')_y - \max_{i \neq y} Z(\mathbf{x}')_i, 0)$, using the iterative crafting process.

ZOO (Chen et al., 2017) has been proposed to optimize Eq. (24) in the black-box manner through queries. It estimates the gradient at each coordinate as

$$\hat{g}_i = \frac{\mathcal{L}(\mathbf{x} + \sigma \mathbf{e}_i, y) - \mathcal{L}(\mathbf{x} - \sigma \mathbf{e}_i, y)}{2\sigma} \approx \frac{\partial \mathcal{L}(\mathbf{x}, y)}{\partial x_i}, \quad (25)$$

where \mathcal{L} is the objective in Eq. (24), σ is a small constant, and \mathbf{e}_i is the i -th unit basis vector. In our experiments, we perform one update with \hat{g}_i at one randomly sampled coordinate. We set $\sigma = 10^{-4}$ and max queries as 20,000.

NES (Ilyas et al., 2018) and **SPSA** (Uesato et al., 2018) adopt the update rule in Eq. (21) for adversarial example

Table 7. Classification accuracy (%) on **CIFAR-10** under the *white-box* threat model. The perturbation $\epsilon = 0.031$, step size $\eta = 0.003$.

Defense	Clean	PGD-20	PGD-500	MIM-20	FGSM	DeepFool	C&W- ℓ_∞
PGD-AT	86.75	53.97	51.63	55.08	59.70	57.26	84.00
PGD-AT + HE	86.19	59.36	57.59	60.19	63.77	61.56	84.07
PGD-AT + m-HE	86.25	59.90	58.46	60.50	63.70	59.47	83.71
ALP	87.18	52.29	50.13	53.35	58.99	59.40	84.96
ALP + HE	89.91	57.69	51.78	58.63	65.08	65.19	87.86
ALP + m-HE	89.23	57.09	53.34	58.04	63.81	60.74	87.21
TRADES	84.62	56.48	54.84	57.14	61.02	60.70	81.13
TRADES + HE	84.88	62.02	60.75	62.71	65.69	60.48	81.44
TRADES + m-HE	84.30	61.83	60.43	62.67	65.49	60.51	80.53

generation. Although the true gradient is unavailable, NES and SPSA give the full gradient estimation as

$$\hat{g} = \frac{1}{q} \sum_{i=1}^q \frac{\mathcal{J}(\mathbf{x} + \sigma \mathbf{u}_i, y) - \mathcal{J}(\mathbf{x} - \sigma \mathbf{u}_i, y)}{2\sigma} \cdot \mathbf{u}_i, \quad (26)$$

where we use $\mathcal{J}(\mathbf{x}, y) = Z(\mathbf{x})_y - \max_{i \neq y} Z(\mathbf{x})_i$ instead of the cross-entropy loss, $\{\mathbf{u}_i\}_{i=1}^q$ are the random vectors sampled from a Gaussian distribution in NES, and a Rademacher distribution in SPSA. We set $\sigma = 0.001$ and $q = 128$ in our experiments, as default in the original papers.

C. More Empirical Results

In this section, we provide more empirical results and setups. In our experiments, we apply NVIDIA P100 / 2080Ti GPUs, as well as the Apex package to execute training for FastAT (Coleman et al., 2017; Wong et al., 2020). On CIFAR-10, all the models are trained by four GPUs in parallel for PGD-AT, ALP, and TRADES.

C.1. Code References

To ensure that our experiments perform fair comparison with previous work, we largely adopt the public codes and make minimal modifications on them to run the trials. Specifically, we refer to the codes of TRADES⁴ (Zhang et al., 2019b), FreeAT⁵ (Shafahi et al., 2019), FastAT⁶ (Wong et al., 2020) and the corrupted datasets⁷ from Hendrycks & Dietterich (2019). The codes are mostly based on PyTorch (Paszke et al., 2019).

C.2. Datasets

The CIFAR-10 dataset (Krizhevsky & Hinton, 2009) consists of 60,000 32x32 colour images in 10 classes, with 6,000 images per class. There are 50,000 training images and 10,000 test images. We perform RandomCrop with 4 padding and RandomHorizontalFlip in training as the data

⁴<https://github.com/yaodongyu/TRADES>

⁵<https://github.com/mahyarnajibi/FreeAdversarialTraining>

⁶https://github.com/locuslab/fast_adversarial

⁷<https://github.com/hendrycks/robustness>

augmentation. The ImageNet (ILSVRC 2012) dataset (Deng et al., 2009) consists of 1.28 million training images and 50,000 validation images in 1,000 classes. As to the data augmentation, we perform RandomResizedCrop and RandomHorizontalFlip in training; Resize and CenterCrop in test. The image size is 256 and the crop size is 224.

C.3. The choices of scale s and margin m in HE

Different choices of the scale s and the margin m in HE lead to different trade-offs between the clean accuracy and the adversarial robustness of the trained models, as shown in Table 8. This kind of trade-off is ubiquitous w.r.t. the hyperparameter settings in different AT frameworks (Zhang et al., 2019b; Kannan et al., 2018).

 Table 8. Classification accuracy (%) on **CIFAR-10**. The training framework is PGD-AT + HE with different scale s and margin m .

Defense	Scale s	Margin m	Clean	PGD-20
PGD-AT + HE	10	0.2	86.77	58.04
	15	0.2	86.19	59.36
	20	0.2	85.32	60.18
	30	0.2	83.30	60.86
	10	0.25	86.52	58.18

C.4. Full Results of m-HE on CIFAR-10

In Table 7, we evaluate the white-box performance of the combinations of the modified HE (m-HE) with PGD-AT, ALP, and TRADES. We set the parameters with $s = 15$ and $m = 0.1$. We can see that m-HE is more effective than HE when combining with PGD-AT, FreeAT and Fast AT that exclusively train on adversarial examples. In contrast, HE performs better than m-HE when combining with the frameworks training on the mixture of clean and adversarial examples, e.g., ALP and TRADES.

C.5. Full Results on CIFAR-10-C and ImageNet-C

In Table 9 and Table 10 we provide the full classification accuracy results of different defenses on CIFAR-10-C and ImageNet-C (Hendrycks & Dietterich, 2019), respectively. These reports include detailed accuracy under 75 combinations of severity and corruption.

Table 9. Classification accuracy (%) on **CIFAR-10-C**. Full results on different combination of severity and corruption.

Defense	Severity	Noise			Blur				Weather				Digital			
		Gauss	Shot	Impulse	Defocus	Glass	Motion	Zoom	Snow	Frost	Fog	Bright	Contra	Elastic	Pixel	JPEG
PGD	1	85.97	86.3	83.55	86.15	81.92	83.65	82.86	86.12	84.88	84.27	87.15	82.37	82.06	86.23	85.17
	2	84.16	85.82	79.92	84.8	82.06	80.09	82.49	84.4	80.84	76.22	86.68	59.77	82.2	85.62	84.64
	3	81.22	83.08	76.79	82.87	81.55	76.32	81.12	82.39	75.24	65.71	85.7	40.64	81.13	85.33	84.41
	4	79.4	81.2	69.55	80.67	76.18	76.39	80.17	78.03	75.93	51.96	83.87	23.09	79.65	84.27	83.86
	5	77.48	78.02	62.8	74.7	76.72	71.66	77.77	75.69	72.9	30.37	76.86	16.9	78.95	82.37	83.69
PGD+HE	1	85.37	85.67	83.7	85.63	81.51	83.75	82.67	85.33	84.26	84.1	86.45	82.43	81.69	85.43	85.05
	2	83.69	84.99	80.97	84.5	81.76	80.66	82.33	83.99	80.33	76.84	86.0	61.36	81.92	85.15	84.52
	3	81.14	82.46	78.01	82.65	81.2	76.73	81.11	81.43	75.71	66.59	85.17	41.76	81.2	84.63	84.05
	4	79.74	81.25	71.67	80.83	76.14	77.03	80.09	77.77	76.35	52.75	83.31	23.65	80.01	83.77	83.67
	5	77.76	77.99	66.37	75.58	76.67	72.68	78.16	75.35	73.28	31.96	77.44	16.36	78.61	81.84	83.23
ALP	1	86.57	86.93	84.13	86.53	83.04	84.12	83.07	86.4	85.77	85.12	87.4	83.21	82.18	86.46	85.79
	2	84.96	86.31	80.48	85.01	82.65	81.04	82.73	84.86	82.19	77.27	87.24	61.34	82.11	86.02	85.09
	3	81.84	83.55	77.23	82.84	81.83	76.91	81.15	82.76	76.57	65.68	86.36	41.96	81.32	85.73	84.63
	4	80.05	81.64	69.53	80.65	77.1	77.09	80.17	78.56	77.54	51.09	84.74	24.92	80.13	84.46	84.23
	5	78.01	78.6	62.97	74.69	76.96	71.99	77.75	76.13	74.26	28.39	78.66	17.85	78.81	82.79	83.68
ALP+HE	1	88.61	89.27	85.56	89.58	83.58	87.05	86.36	88.71	88.62	88.2	90.1	86.55	85.93	89.37	88.52
	2	85.89	88.25	81.13	88.15	83.79	83.83	85.88	87.0	86.2	82.37	89.9	69.33	85.97	88.72	87.62
	3	81.61	83.99	76.29	86.14	83.69	79.81	84.68	85.71	82.47	73.58	89.13	51.2	84.94	87.98	86.99
	4	78.72	81.42	67.61	84.08	75.73	80.34	83.73	82.52	82.79	61.5	88.06	30.06	83.36	86.92	86.89
	5	76.26	76.64	60.84	78.21	77.56	75.28	81.5	81.76	79.36	38.48	84.46	16.58	82.01	84.19	86.37
TRADES	1	83.74	84.16	81.61	84.01	79.97	81.98	80.69	84.16	83.57	82.53	85.21	79.91	79.47	84.22	83.27
	2	81.84	83.44	78.34	82.61	79.85	78.62	80.04	82.96	79.7	74.42	84.78	57.63	79.8	83.45	82.64
	3	78.63	80.56	74.84	80.58	79.55	75.09	78.9	80.79	73.97	63.06	83.78	39.34	79.05	83.07	82.32
	4	77.09	78.42	67.85	78.62	74.7	75.0	77.9	76.33	75.08	49.91	82.13	24.6	77.48	82.2	81.83
	5	74.8	75.27	61.88	73.4	74.55	71.03	75.78	73.39	72.41	28.5	74.41	17.54	76.86	80.31	81.53
TRADES+HE	1	83.06	83.78	81.12	83.96	79.42	82.13	81.28	83.69	83.22	82.31	85.0	80.2	80.35	83.84	83.24
	2	81.18	83.02	78.41	82.89	79.75	79.39	81.03	82.23	79.21	75.12	84.93	60.38	80.14	83.23	82.64
	3	78.43	80.11	75.4	81.35	79.53	76.19	79.9	80.13	73.93	65.6	83.87	41.97	79.88	83.12	82.37
	4	76.85	78.63	69.59	79.78	74.03	76.62	78.95	76.34	74.51	52.36	82.2	25.59	78.33	82.16	82.07
	5	74.89	75.55	64.55	74.77	75.32	71.98	76.92	73.74	71.79	31.56	75.64	17.07	77.74	80.17	81.66

 Table 10. Classification accuracy (%) on **ImageNet-C**. Full results on different combination of severity and corruption..

Defense	Severity	Noise			Blur				Weather				Digital			
		Gauss	Shot	Impulse	Defocus	Glass	Motion	Zoom	Snow	Frost	Fog	Bright	Contra	Elastic	Pixel	JPEG
FreeAT	1	54.26	53.23	44.00	33.91	42.25	43.97	38.64	42.57	45.83	11.00	56.42	18.29	48.45	53.91	54.74
	2	45.84	43.08	32.60	26.68	34.06	34.70	33.36	26.16	28.50	4.41	53.20	6.59	31.78	52.98	53.92
	3	29.74	28.36	23.48	16.82	25.22	23.83	26.93	22.69	17.22	1.54	47.98	1.38	49.64	50.19	53.34
	4	12.96	10.66	8.91	11.10	19.35	15.20	23.52	11.98	15.51	1.20	39.56	0.40	46.09	45.24	51.57
	5	3.28	4.85	2.73	7.25	12.29	11.05	18.84	11.75	10.28	0.43	28.73	0.34	32.82	41.55	49.19
FreeAT+HE	1	55.14	53.27	44.29	38.15	46.08	47.57	41.90	45.92	50.32	15.25	58.73	23.31	51.15	56.17	57.03
	2	43.96	40.02	29.08	30.34	37.97	38.39	36.21	30.21	34.26	6.59	56.47	9.23	34.61	55.40	56.23
	3	24.49	23.14	18.38	18.52	27.98	26.44	29.38	26.83	22.34	2.39	52.39	1.71	52.64	52.65	55.77
	4	9.37	8.37	5.89	11.71	21.45	16.42	25.61	15.22	20.43	1.85	45.56	0.47	48.94	47.82	54.17
	5	2.23	3.95	1.63	7.09	12.93	11.59	20.68	14.89	14.36	0.58	36.21	0.41	36.25	43.81	52.04